Late Cretaceous-Eocene exhumation of the northern Lhasa terrane and topographic implications for the Central Tibet

Late Cretaceous-Eocene exhumation of the northern Lhasa terrane and topographic implications for the central Tibet

Gaoyuan Sun[a, b, *], Hugh D. Sinclair[c], Cristina Persano[d], Finlay M. Stuart[e] and Xiumian Hu[b*]

[a] College of Oceanography, Hohai University, Nanjing, 210024, China;

[b] State Key Laboratory for Mineral Deposits Research, School of Earth Sciences and Engineering, Nanjing University, Nanjing 210023, China;

[c] School of GeoSciences, University of Edinburgh, Edinburgh EH8 9XP, UK;

[d] School of Geographical and Earth Sciences, University of Glasgow, Glasgow G12 8QQ UK;

[e] Scottish Universities Environmental Research Centre, East Kilbride G75 0QF, UK.

[*]Correspondence: Sun, G.Y., sungy@hhu.edu.cn; Hu, X.M., huxm@nju.edu.cn

Keywords

Low-temperature thermochronology; Synchronous exhumation; Plateau growth; Relief

Abstract

The central Tibetan Plateau has an average altitude of ~5000 m; its exhumation and chemical weathering greatly influence the global climate and ocean chemistry. The modern central Tibet is characterized by low-relief, high elevation topography with endorheic drainage. When and how these geomorphic characteristics of central Tibet were initiated remains controversial. Here, we have applied zircon U-Pb dating and low-temperature thermochronology on the Cretaceous plutons from Coqin Basin of central Tibet in order to assess timings of exhumation. The thermal history modeling indicates a period of relatively rapid cooling (2.5-4°C/Ma) occurred in Late Cretaceous to Middle Eocene times (from ~80 Ma to ~40 Ma), with the exhumation rates of 0.2-0.4 mm/yr assuming a geothermal gradient of 25°C/km. Cooling rates then slowed to ~0.5°C/Ma during the Middle Eocene to the present, with a relatively lower exhumation rates of ~0.02-0.03 mm/yr. Synchronous rapid cooling and exhumation has also been identified in central Tibet; this signal of widespread Late Cretaceous exhumation across the region may be viewed as evidence for the initial surface uplift and erosion of the central Tibetan plateau. Lower exhumation rate since ~40 Ma, combined with sedimentological data suggests that the low-relief, internally drained topography of central Tibet was initiated around this time.

1. Introduction

The timing of structural and topographic growth of the Tibetan Plateau is significant for understanding the geodynamics of plateau uplift and its implications for global climate change (An et al., 2001). The modern central Tibet (mostly including the northern Lhasa and Qiangtang terranes) is characterized by low-relief, high elevation topography which is internally drained (Han et al., 2019, Xue et al., 2022). The inception and development of these geomorphic characteristics in central Tibet remain controversial. One perspective proposes a “peneplain” model involving planation processes driven by an external river system near sea-level on the central Tibetan Plateau prior to the India-Asia collision (Hetzel et al., 2011). In contrast, other studies argue that the plateau growth was initiated in Late Cretaceous time and the high elevation was gained by Eocene times (Rohrmann et al. 2012; Dai et al., 2013). However, the paleo-

elevation data indicate that central Tibet has undergone a complex history of surface uplift, with formation of the Late Cretaceous protoplateau and subsequent collapse to the "Central Tibetan Valley" in the Paleocene (Hu et al., 2020; Xiong et al., 2022). Furthermore, formation of low-relief topography across central Tibet was asynchronous due to an endorheic drainage system reducing high-elevation ranges to fill local basins within the plateau (Liu-Zeng et al., 2008). Consequently, significant uncertainty exists about the topographic evolution history, concerning the timing of structural growth of the plateau and relief conditions on the central Tibet.

The evolution of topographic relief relates to rates of surface uplift through changes in rates of river incision relative to hillslope response (Montgomery, 1994). So relief is more directly linked to rock uplift and exhumation than to absolute elevation (England and Molnar, 1990). Hence assessing rock exhumation serves as an approximation for investigating topographic evolution. Low-temperature thermochronology techniques such as zircon/apatite fission track and U-Th-He are employed to determine rock cooling histories, thereby approximating rock exhumation. A few studies from the eastern part of central Tibet (i.e., from Baingoin to Nima regions, Fig. 1) have reported rapid cooling and exhumation before ~45-30 Ma (Rohrmann et al. 2012; Dai et al., 2013; Xue et al., 2022). However, data is scarce for constraining the exhumation history in the vast western segment of central Tibet. In Gaize region of the BNSZ, a multistage exhumation history has been discovered based on data from the clastic succession, showing three cooling stages of 120-100 Ma, 85-55 Ma and 47-30 Ma (Li et al., 2022, Tong et al., 2022). The structural reconstruction in the western part of central Tibet shows substantial crustal deformation with nearly 50% shortening (Murphy et al., 1997; Kapp et al., 2003, 2005, 2007; Volkerman et al., 2007), implying that surface uplift corresponding to Late Cretaceous crustal shortening may have occurred along with similar exhumation history as shown in eastern parts of central Tibet. Thus, examining bedrock exhumation history from the west segment of central Tibet will test models of thermal development and hence interpretations of the topographic growth across the entire central Tibetan Plateau.

The Coqin Basin, situated in the west part of northern Lhasa terrane, is bound by the Gangdese magmatic arc to the south and the Bangong-Nujiang suture zone (BNSZ) to the north

(Fig. 2). The basin comprises a thick Mesozoic to Cenozoic succession intruded by Cretaceous plutons. In order to better constrain the exhumation history of the west segment of the central Tibet, we apply zircon U-Pb dating and low-temperature thermochronology to Cretaceous plutons in the Coqin Basin, which, combined with the stratigraphic record, yield insights into the thermal history of this critical portion of the Tibetan Plateau. By comparing with previous studies, a synchronous exhumation history spanning Late Cretaceous-Middle Eocene is reconstructed for central Tibet. Based on the results, we suggest that the low-relief, internally drained aspects of the central Tibet were established since the Middle Eocene (~40 Ma).

2. Geological setting and study area

The Lhasa terrane is separated from the Tethys Himalaya by the Yarlung-Zangbo suture to the south and from the Qiangtang terrane by the Bangong-Nujiang suture to the north (Fig. 1a, Kapp and DeCelles, 2019). The Lhasa terrane has two parts, including the southern and northern Lhasa (Fig. 2a, Burg et al., 1983). The southern Lhasa terrane contains the Gangdese magmatic arc and Xigaze forearc basin. The Gangdese magmatic arc is mainly composed of the Late Triassic-Early Cenozoic Gangdese batholiths and Cenozoic Linzizong volcanic rocks (Ji et al., 2009; Zhu et al., 2011). The Xigaze forearc basin, located on the southern margin of the Gangdese magmatic arc, is featured as the thick sequences of Albian-Campanian deep-water turbidites (Wang et al., 2012). The northern Lhasa terrane includes substantial Cretaceous magmatic rocks (e.g., the Zenong volcanism, Zhu et al., 2006, 2009) and more than 5-km-thick sedimentary rocks (such as the Mesozoic sedimentary basins of Coqin and Nima, Kapp et al., 2007; Sun et al., 2015a, 2017). Structural reconstruction of the Lhasa terrane demonstrates the substantial crustal deformation and shortening in Cretaceous time, with approximately ~50% north-south shortening over the modern Lhasa terrane (Li et al., 2015 and references therein).

The Coqin Basin (Fig. 2b), located in the west of the northern Lhasa terrane, accumulated more than 3000 m of Cretaceous strata, i.e., Duoni, Langshan and Daxiong formations. The Lower Cretaceous Duoni and Langshan formations were deposited in marginal-shallow marine environments, that accumulated both clastic and carbonate successions respectively (Xu et al., 2022). The Upper Cretaceous (~90 Ma) Daxiong conglomerate overlies the Langshan limestones

104 with an unconformity or the southward thrust (Sun et al., 2015a). After a hiatus from Late
105 Cretaceous to Early Eocene times (i.e., ~90-40 Ma), the Eocene lacustrine Dingqinghu Formation
106 (>1300 m-thick) was deposited with the unconformity above the underlying strata. The Cretaceous
107 granitic plutons were intruded into the sedimentary sequence in the basin. The structural
108 deformation mainly occurred in Late Cretaceous to Eocene times in the Coqin Basin (Li et al.,
109 2015). There were two oppositely vergent thrust belts in Late Cretaceous time: the north-dipping
110 Coqin thrust and the south-dipping Gaize-Selin Co thrust (Fig. 1b), which combined resulted in
111 ~250 km crustal shortening between ~100-50 Ma (Murphy et al., 1997; Kapp et al., 2007; Li et al.,
112 2015).

113 ## 3. Sampling and methods

114 The low-temperature thermochronology data were obtained from eight samples, collected
115 from the Coqin Basin (Fig. 2b). Three samples (XL01-03) were collected from the Xialong biotite
116 granodiorite plutons in the northern part of the Coqin Basin. The other five samples are from the
117 Chaji Co and Jiangrang Ruoyu plutons in the southern Coqin Basin. All these pluton samples were
118 collected on a low-relief plateau surface away from the modern active faults.

119 Zircon and apatite grains were separated by crushing, grinding and then concentrated using
120 standard heavy liquid and magnetic separation techniques. Zircon U-Pb dating of three granitoids
121 (CJ03, DX102 and XL02) from the Chaji Co, Jiangrang Ruoyu and Xialong pluton bodies, were
122 conducted at the State Key Laboratory for Mineral Deposits Research, Nanjing University, China,
123 using a laser ablation inductively coupled plasma mass spectrometry (LA-ICP-MS). More details
124 of the instrumental conditions and analytical procedures are outlined in Liu et al. (2013). The
125 primary Pb isotopic data were calculated and exported by GLITTER 4.4 software (van
126 Achterbergh et al., 2001) and common Pb corrections followed the program by Andersen (2002).
127 The weighted mean ages were obtained using the Isoplot/Ex program (version 2.49) of Ludwig
128 (2001). The uncertainties in the single grain and weighted mean ages, including all known
129 systematic errors, are cited at the 1σ and 2σ levels, respectively. The ages obtained of this study
130 exclude analyses with >20% discordance.

Zircon and apatite (U-Th)/He (ZHe and AHe) analyses were conducted in the Scottish Universities Environmental Research Centre. Euhedral, unfractured, large and optically inclusion-free zircon and apatite grains were selected. The digitized photographs were taken for measuring the geometric parameters to calculate the α-ejection corrections. Each single zircon and apatite grain was encapsulated in a platinum tube and loaded into a stainless steel capsule. Helium concentration was measured by a 99.9% pure 3He spike in a Hiden HAL3F quadrupole mass spectrometer equipped with an electron multiplier detector. After measurement, each capsule was retrieved and dissolved in ^{235}U- and ^{230}Th spiked nitric acid. U and Th concentrations were measured using a VG PlasmaQuad 2 ICP-MS. The detailed procedures can be found in Foeken et al. (2006) and Dobson et al. (2008).

The apatite fission track (AFT) determinations were made in the laboratory of School of Geographical and Earth Sciences, University of Glasgow, UK. The fission track ages, track lengths, and Dpar measurements were carried out with the external detector method (Gleadow, 1981; Hurford and Green, 1982) and the zeta calibration technique (Hurford and Green, 1983). The spontaneous and induced fission tracks were counted on a Zeiss Axioplan microscope with a 100× dry objective and a total magnification of 2000×. About 20 grains of each sample were identified for AFT age determination. Track lengths and Dpar were measured at 2000× magnification and were measured on the same grain with age dating. More details about the measurements of AFT can be found in Persano et al. (2005).

4. Results

Zircon U-Pb dating from samples CJ03 and DX102 yield ages of 115.1 ± 1.4 Ma and 111.7 ± 0.7 Ma, respectively, while sample XL02 from the northern part of the Coqin Basin shows a Late Cretaceous age of 92.1 ± 0.5 Ma (Fig. 3, Supplementary table S1).

The samples from the northern part of the Coqin Basin (XL01-03) give ZHe weighted mean recoil-corrected ages ranging 70.9 ± 0.7 Ma to 88.2 ± 0.9 Ma. Five samples from the southern part (CJ01, CJ03, DX02, DX101, and DX102) yield ZHe mean ages that range from 54.4 ± 0.6 Ma to 69.8 ± 0.7 Ma. AFT analyses of five granites (CJ01, DX02, XL01-03) yield ages of 53.9 ± 4.0 Ma

158 to 75.0 ± 7.4 Ma. Non-projected mean track lengths of these samples are between 13.0 and 14.9
159 μm with standard deviations around 1.1 μm, indicative of rapid cooling through the partial
160 annealing zone. Samples XL01-03 from the northern part of the basin give weighted mean AHe
161 ages of 70.6 ± 0.9 Ma, 62.6 ± 0.8 Ma 58.8 ± 1.1 Ma, respectively, while the other five samples
162 from the south (CJ01, CJ03, DX02, DX101, and DX102) produce the younger ages, with the
163 weighted mean ages of 45.1 ± 2.1 Ma to 56.4 ± 0.6 Ma. The detailed age information can be
164 referred to the Table 1, and Supplementary table S2-3.

165 # 5. Thermal history modeling

166 ## 5.1 Modeling strategy

167 Single-sample thermal histories were modelled using HeFty software (Ketcham 2005) using
168 the ZHe, AHe and AFT data. The Dpar value for each sample was used during the AFT modeling,
169 and the multi-kinetic annealing model (Ketcham et al., 2007) was applied. The radiation damage
170 accumulation and annealing model (RDAAM) for helium diffusion in apatite (Flowers et al.,
171 2009), and the diffusion kinetics of Reiners et al. (2004) were used for modeling AHe and ZHe
172 single-grain ages. Key geological constraints were employed in the thermal history modeling.
173 These included 1) present-day surface temperature of 10 ± 10°C, 2) initial time-temperature
174 constraint was set at 220-170°C, and 3) a broad temperature span (i.e. 230-120°C for the weight
175 mean ZHe age and 80-40°C for weight mean AHe age) was set to constrain the cooling path.
176 These pre-modeling settings were always included with a large uncertainty so as to give the
177 modeling enough freedom to search for a wide range of data-constrained thermal histories.

178 ## 5.2 Results of thermal history modeling

179 Five samples (XL01-03, CJ01 and DX02) yielded compatible ages when ZHe, AFT and AHe
180 data were employed together for the thermal-kinetic modeling (Fig. 4). For the other three samples
181 (CJ03, DX101 and DX102), there are few induced fission tracks obtained when conducted the
182 AFT analysis, thus these three samples were modelled with ZHe and AHe data. All samples reveal
183 that there was a rapid cooling history from Late Cretaceous (~80-75 Ma) to Eocene (~40 Ma)
184 times followed by a period of slow cooling. It is difficult to quantify the precise exhumation rates,

because of the influences of local topography and paleogeothermal gradient. However, the initial exhumation history of the northern Lhasa can be determined based on the data obtained in this study. The ZHe ages are within error of the AFT and AHe ages, suggesting rapid exhumation in Late Cretaceous times. To better quantify the exhumation history, inverse thermal history modeling was employed based on a combination of ZHe, AFT and AHe data. The results of thermal history modeling are plotted in Fig. 5. The results confirm that there was a rapid cooling history from ~80 Ma (Late Cretaceous time) to 45 Ma followed by a period of slow cooling.

6. Discussion

6.1 The Late Cretaceous-Middle Eocene cooling history in Coqin Basin

Two samples (CJ03 and DX102) from the Chaji Co and Jiangrang Ruoyu plutons in the southern region of Coqin Basin, yield the zircon U-Pb ages of 115.1 ± 1.4 Ma and 111.7 ± 0.7 Ma, respectively. The hornblende and K-feldspar from the plutons produce the $^{40}Ar/^{39}Ar$ isochron age of ~99-92 Ma (Murphy et al., 1997). Both of the U-Pb and $^{40}Ar/^{39}Ar$ data indicate rapid Early-mid Cretaceous cooling (22.5°C/Ma) from zircon crystallization temperature (~800°C) to ~350°C within ~20 Ma, which could be best interpreted by the magma cooling following its emplacement. These processes are consistent with the pluton emplacement at mid-crustal levels into the Lower Cretaceous strata by ~99-92 Ma (Murphy et al., 1997). All samples from these two plutons (samples CJ01, CJ03, DX02, DX101 and DX102), yield multi-system thermochronometers with the overlapped ages of ~75-40 Ma among the average zircon He ages, and Apatite He and fission track ages. These low-temperature thermochronometers indicate rapid cooling in Late Cretaceous to Middle Eocene time. The rapid cooling of plutons could be induced by the quick erosion of overlying rocks or the thermal equilibration to the country rocks during the magma emplacement. After the Early-mid Cretaceous emplacement, these plutons have undergone an accelerated cooling from the Late Cretaceous to Middle Eocene time according to the thermal history modeling based on the above low-temperature data. This accelerated cooling is interpreted as the result of erosion of overlying rocks and pluton exhumation, which is consistent with the timing of displacement linked to the Coqin thrust (~100-50 Ma), that transported the plutons over the

hanging wall (Fig. 1b, Murphy et al., 1997; Volkman et al., 2007). Similarly, the erosion of the overlying rocks can be also certified by the contemporary sedimentary records in the Coqin Basin. The Upper Cretaceous conglomerates (Daxiong Formation) had accumulated in the footwall of the Coqin thrust and received the sediments from the local topographic highs (Sun et al., 2015a).

Three samples (XL01-03) from the Xialong plutons in the northern part of the Coqin Basin, give the same zircon U-Pb and He ages of ~ 90 Ma within uncertainties, indicating the rapid magma cooling and thermal equilibration to the country rock during their emplacement. The thermal history modeling based on the apatite fission track and He ages, yield a quick cooling (~3°C/Ma) between 80 Ma to 50 Ma, which falls within the time span of activity on the Gaize-Selin Co thrust in the northern margin of northern Lhasa terrane (i.e., 100-25 Ma, Kapp et al., 2007).

Overall, our new thermochronometric data of these Cretaceous plutons from the Coqin Basin, yield a rapid Late Cretaceous-Eocene (from ~80 Ma to as late as ~40 Ma) cooling of 2.5-4°C/Ma, representing a denudation rate of approximately 0.2-0.4 mm/yr assuming a geothermal gradient of 25°C/km (Fig. 5). Since ~40 Ma, the cooling rate has slowed down to ~0.5°C/Ma, with the denudation rate of ~0.02-0.03 mm/yr. This Late Cretaceous rapid cooling event has coincided with the activation of two thrust system in the Coqin Basin. In consideration of the positions of pluton bodies, the Chaji Co-Jiangrang Ruoyu and Xialong plutons are located on the ramp of thrusts, showing no more than 30 km away from the Coqin thrust to the south and to the Gaize-Selin Co thrust to the north, respectively (Fig. 2). The possible interpretation is that the Late Cretaceous movement on the north-dipping Coqin thrust and the south-dipping Gaize-Selin Co thrusts are responsible for the rapid exhumation of these rocks.

6.2 The synchronous Late Cretaceous exhumation on the central Tibet

Within the northern Lhasa terrane and BNSZ, lots of thermochronologic data derived from the Baingion, Nima and Gaize regions exhibit ZHe ages of ~100-54 Ma, AFT ages of ~88-30 Ma, and AHe ages of ~78-20 Ma (Hetzel et al., 2011; Rohrmann et al., 2012; Haider et al., 2013; Li et al., 2022; Xue et al., 2022). Thermal history modeling suggests that the northern Lhasa terrane and

the BNSZ have a rapid cooling and exhumation history since ~85-70 Ma followed by a slow cooling since ~45-30 Ma (Rohrmann et al., 2012; Xue et al., 2022, Fig. 6). This thermal history modelling result is consistent with our newly obtained low-temperature thermochronologic data in the Coqin Basin. Thermochronologic data derived from both the northern Lhasa terrane and BNSZ suggest regionally synchronous rapid exhumation across central Tibet during the Late Cretaceous-Middle Eocene time (80-40Ma) (Fig. 6). A similar cooling pattern was observed in southern Qiangtang terrane where most ZHe ages spanned approximately ~150 -80Ma, AFT ages ranged between ~95-44 Ma, and AHe ages are of ~85-40 Ma (Zhao et al., 2017; Yang et al., 2019; Qian et al., 2021; Xue et al., 2022). Thermochronological modelling based on these data indicates at least two episodic rapid exhumations at the Late Jurassic and the Late Cretaceous times, respectively (Yang et al., 2019; Qian et al., 2021).

This synchronous cooling history indicates that the interior of Tibet has undergone a relatively uniform exhumation between the Late Cretaceous and Middle Eocene time. The mechanism responsible for this synchronicity warrants further exploration. One plausible explanation could be the underthrusting of Indian lithosphere beneath Lhasa terrane, resulting in significant deformation (DeCelles et al., 2002). This process aligns with the exhumation within the Lhasa terrane. However, it fails to interpret the synchronous exhumation history within the BNSZ and the southern Qiangtang terrane, due to the underthrusting of Indian lithosphere is limit to the Lhasa terrane only (Nábělek et al. 2009). In consideration of the tectonic background, the Lhasa-Qiangtang collision has been widely inferred to have occurred in the Late Jurassic to Early Cretaceous times (Kapp et al., 2007; Ma et al., 2017), which provides an alternative potential mechanism. Under this broad continent-continent collision, abundant upper crustal deformation and shortening occurred in the BNSZ and the surrounding regions. Structural reconstructions indicate that it has accommodated at least ~250 km south-north shortening prior to India-Asia collision (Kapp et al., 2005; Li et al., 2015). As the response, the crust below the Lhasa-Qiangtang collision zone has experienced significant thickening.

6.3 The initial growth of the central Tibet

The previous low-temperature thermochronometers from central Tibet have revealed the rapid exhumation and surface elevation gain during the Cretaceous to Eocene times (Rohrmann et al., 2012, Dai et al., 2013). Here, combined with the previous and this low-temperature thermochronology studies, we propose that the rapid Late Cretaceous-Middle Eocene exhumation resulted from initial surface uplift due to crustal thickening and shortening within the Lhasa-Qiangtang collision zone. A few additional lines of geological evidence can contribute to this interpretation: Firstly, since ~90 Ma, the entire northern Lhasa terrane has recorded a sharp environmental change from marine limestone deposits to terrestrial alluvial conglomerates (Sun et al., 2015a; Lai et al., 2019). Secondly, a significant ~90 Ma episode of magmatism developed on the northern Lhasa terrane indicative of crust thickening (Wang et al., 2014; Sun et al., 2015b). Thirdly, there are no sedimentary records on the northern Lhasa terrane between mid-Cretaceous to Eocene times (Fig. 7), and so the northern Lhasa terrane served as the erosional source at that time. When considering this over the broader region of central Tibet, previous studies proposed that the Tibetan plateau growth originated from plateau interior before expanding southwards and northwards (Wang et al., 2008).

The low-temperature thermochronometers of this study, alongside the geological evidence strongly indicates that the initial surface growth occurred in central Tibet from Late Cretaceous (at least at ~80 Ma). However, the clumped isotopic data from the Lunpola Basin reveal a "Central Tibetan Valley" existed in the BNSZ during ~50-40 Ma (Fang et al., 2020; Xiong et al., 2022). Similarly, a low elevation condition in the Gaize Basin during the Eocene time has been reconstructed by foraminifera and stable isotopes (Wei et al., 2016). Therefore, it is likely that the growth of central Tibet was initiated in the Late Cretaceous, coupled with the river incision. The eroded detritus has been transported along the "Central Tibetan Valley" of the BNSZ by the external drainage systems.

6.4 The topographic implications for the central Tibet

Low-relief landscapes tend to be associated with low denudation rates (e.g., Liu-Zeng et al., 2008; Tian et al., 2014). In contrast, the accelerated exhumation/denudation rate suggests a high-relief landscape. The modern low-relief landscape at high elevations on the central Tibet must

have undergone surface uplift and a reduction of topographic relief. If a high-relief landscape has remained for a prolonged time, the surface exhumation rate should be sustained to a relatively high level (e.g., Clark et al., 2005; Tian et al., 2014). Our data indicate that the rapid cooling history during the Late Cretaceous-Middle Eocene time, coupled with river incision in central Tibet, aligns with the high-relief landscape conditions. The Eocene to present limited cooling rate (~0.5°C/Ma) following the Late Cretaceous rapid cooling (2-3°C/Ma), is probably associated with the formation of a low-relief landscape in the central Tibet (initiated at ~40 Ma). Consequently, we interpret that from middle Eocene times (~40 Ma) to present, the low-relief landscape would have been established, so that the prolonged low cooling rate (~0.5°C/Ma) has prevailed in central Tibet (Rohrmann et al., 2012, Dai et al., 2013).

The provenance data reveal that the Upper Cretaceous Daxiong and Jingzhushan formations on the northern Lhasa terrane (~96-90 Ma) have uniquely sourced from the northern Lhasa terrane by alluvial and braided rivers (Sun et al., 2015a). Since then, it is remarkable that there are no sedimentary records during ~90-40 Ma in the central Tibet (Fig. 7), which could demonstrate external drainage to other basins or to the ocean (Xue et al., 2022). Laskowski et al. (2019) suggests the ancestral Lhasa River has originated from the northern Lhasa terrane and drained across the Gangdese mountains to the south during the Late Cretaceous time (~80 Ma). Within this external drainage system, the northern Lhasa terrane-sourced detritus would have been delivered to the external basins, such as the Xigaze forearc basin in the Neo-Tethyan ocean to the south (An et al., 2014; Orme et al., 2015; Orme and Laskowski, 2016). It is assumed that the Paleocene-Eocene "Central Tibetan Valley" in BNSZ served as a narrow and relatively low-elevation region where the external drainage system from northern Lhasa and Qiangtang terranes were discharged. This topographic evolution in central Tibet could possibly be interpreted as part of a more complex surface uplift history of Tibetan Plateau, with the existence of a Late Cretaceous protoplateau and subsequent collapse (Hu et al., 2020). Since Middle Eocene times (~40 Ma), the terrestrial lacustrine Dingqinghu Formation had been deposited in the central Tibet (e.g., Nima and Lunpola Basins). The sedimentary aggradation and provenance analyses reveal the transporting patterns for the Dingqinghu Formation are similar to the modern drainage systems, with sources from the central Tibet interior, which suggest that the internal drainage system has

been developed at this time (Han et al., 2019; Xue et al., 2022). In combination with the lower exhumation rates since ca. 40 Ma, it is tentatively suggested that a low-relief, internally drained landscape in central Tibet, was initiated before the Middle Eocene time (~40 Ma) (Fig. 7).

7. Conclusions

A combination of zircon and apatite (U-Th)/He and apatite fission track data has been obtained from central Tibet, and thermal history models of these data show a phase of rapid cooling during the Late Cretaceous-Eocene time (from ~80 Ma to as late as ~40 Ma). It is inferred that initial surface uplift and erosion linked to displacement on key thrusts accounts for this synchronous rapid cooling on the central Tibet. Lower exhumation rates since ca. 40 Ma combined with sedimentological evidences suggests that the lower relief, internally drained aspects of the region were initiated around this time.

Acknowledgments

We sincerely thank Katarzyna Luszczak and Luigia Di Nicola for their help on the AFT, ZHe and AHe analyses in thermochronology laboratories of University of Glasgow and Scottish Universities Environmental Research Centre. This study was financially supported by the National Key R & D Program of China (2022YFF0800800) and the National Natural Science Foundation of China (Grant No. 42072124). We thank Dr. Z-B Zhao and one anonymous reviewer for constructive comments that have improved the quality of this manuscript and the editor for comments and editorial handling.

Figure and Table captions

Fig. 1 (a) Tectonic framework of the Tibetan plateau. (b)Topographic map of the Tibetan Plateau Showing the low-temperature data compiled from Hetzel et al., 2011; Rohrmann et al., 2012; Haider et al., 2013; Zhao et al., 2019; Yang et al., 2019; Qian et al., 2021; Li et al., 2022; Xue et al., 2022; Tong et al., 2022. JSSZ—Jinsha suture zone; BNSZ—Bangong-Nujiang suture zone; IYSZ—Indus-Yarlung suture zone.

Fig. 2 Geological map of the Coqin Basin and the related intrusive plutons (Liu et al., 2004), and sampling locations.

Fig. 3 U-Pb plots for samples CJ03, DX102, and XL02. The left are concordant plots and the right are weighted average ages.

Fig. 4 Single-sample thermal kinetic modeling results and the distribution of the measured samples. Refer to the text for the modeling strategy. The pink area in each plot displays the envelope of all good time-temperature paths with goodness of fit (degrees of match between observations and modeled results for both age and length) > 0.6, whereas the green area depicts the envelop for all acceptable time-temperature paths with goodness of fit > 0.05. The thick blue boxes are defined by zircon and Apatite (U-Th)/He ages of samples and their respective closure temperatures. The thick black line in each plot represents the best fit thermal history, with goodness of fit > 0.95.

Fig. 5 Integrated cooling history for the Cretaceous plutons in the Coqin Basin and the geologic events in the Lhasa terrane. Red dots indicate inflections points showing decreases in cooling rate.

Fig. 6 The W-E striking transect of the central Tibetan Plateau with elevations and thermochronologic ages. The topographic profile A-A' and data resources are referred to figure 1b, on which low-temperature thermochronologic ages from 84°E to 92°E are plotted.

Fig. 7 Chronostratigraphic figure of the Coqin Basin from Cretaceous to Miocene times; and the stratigraphic comparison on the northern Lhasa terrane and BNSZ. Sources from Sun et al., (2015a, 2017), and Xue et al., (2022). Relative cooling rates based on thermochronology from this study in the Coqin Basin, Xue et al (2022) in Nima area, Hetzel et al. (2011) and Rohrmann et al. (2012) in Baingoin area, are plotted (black: high cooling rate; gray: low cooling rate). Timing of thrust activity on the two main bounding thrusts are also plotted.

Table 1 Sample location and results of apatite fission track analysis

Sample No.	Lithology	Locality	Elevation	Grains	$\rho_s/\times10^5 cm^{-2}$(Ns)	$\rho_i/\times10^5 cm^{-2}$(Ni)	$\rho_d/\times10^5 cm^{-2}$(Nd)	Length (μm) /No.	P(χ)2	Dpar (μm)	Age (Ma)
CJ01	Biotite monzogranite	31°10′23.7″N 85°26′28.9″E	4734 m	20	5.95(262)	11.1(491)	8.83(5402)	13.0±1.5/20	0.13	2.5	75.0 ±7.4
CJ03	Biotite monzogranite	31°10′23.7″N 85°26′28.9″E	4734 m	-	-	-	-	-	-	-	-
DX02	Biotite monzogranite	31°24′0.5″N 84°58′17.1″E	4834 m	20	8.50(1366)	20.2(3252)	9.02(5520)	14.9±1.1/50	0.00	4.2	60.3 ±4.3
DX102	Monzo granite	31°27′16.9″N 84°59′8.4″E	4850 m	-	-	-	-	-	-	-	-
DX101	Monzo granite	31°23′52.3″N , 84°59′14.2″E	4782 m	-	-	-	-	-	-	-	-
XL01	Biotite granodiorite	31°49′38.6″N 84°34′36.6″E	4741 m	20	6.38(868)	16.9(2298)	8.95(5481)	13.7±1.2/60	0.03	3.0	53.9 ±4.0
XL02	Biotite granodiorite	31°49′38.6″N 84°34′36.7″E	4741 m	20	8.92(949)	19.7(2097)	9.15(5599)	13.2±1.3/25	0.01	2.1	65.9 ±4.9
XL03	Biotite granodiorite	31°51′30.9″N 84°33′53.8″E	4679 m	20	6.86(614)	13.8(1238)	9.21(5639)	13.7±1.4/25	0.08	2.2	72.7 ±5.8

P(χ)2 value of the chi-square age homogeneity test

Dpar measurements are etch pit diameters used as a proxy for the influence of chemical composition on track annealing

Supplementary materials

Supplementary Table S1 LA-ICPMS Zircon U-Pb age dating results

Supplementary Table S2 Results of single-grain zircon U-Th-He dating

Supplementary Table S3 Results of single-grain apatite U-Th-He dating

References

An, W., Hu, X., Garzanti, E., Marcelle, M.K., Wang, J., and Sun, G., 2014, Xigaze Forearc Basin (South Tibet) revisited: Unroofing of the Gangdese arc and origin of the Xigaze ophiolite: Geological Society of America Bulletin, v. 126, p. 1595-1613.

An, Z.S., Kutzbach, J.E., Prell, W.L., and Porter, S.C., 2001, Evolution of Asian monsoons and phased uplift of the Himalaya–Tibetan Plateau since Late Miocene times: Nature, v. 411, p. 62–66, doi: 10 .1038 /35075035.

Andersen, T., 2002, Correction of common lead in U-Pb analyses that do not report ^{204}Pb: Chemical Geology, v. 192, p. 59-79.

Burg, J.P., Proust, F., Tapponnier, P., and Chen, G.M., 1983, Deformation phases and tectonic evolution of the Lhasa block, China: Eclogae Geologicae Helvetiae, v. 76, p. 643–665.

Clark, M. K., M. A. House, L. H. Royden, K. X. Whipple, B. C. Burchfiel, X. Zhang, and W. Tang, 2005, Late Cenozoic uplift of southeastern Tibet: Geology, 33(6), 525–528.

Dai, J., Wang, C., Hourigan, J., & Santosh, M., 2013. Insights into the early Tibetan Plateau from (U–Th)/He thermochronology. Journal of the Geological Society, 170(6), 917-927.

DeCelles P G, Robinson D M, Zandt G., 2002, Implications of shortening in the Himalayan fold-thrust belt for uplift of the Tibetan Plateau. Tectonics, 21(6): 12-1-12-25.

Dobson, K.J., Stuart, F.M., Dempster, T.J., and EIMF, 2008, U and Th zonation in Fish Canyon Tuff zircons: Implications for a zircon (U–Th)/He standard: Geochimica et Cosmochimica Acta, v. 72(19), p. 4745-4755.

England, P. and Molnar, P., 1990, Surface uplift, uplift of rocks, and exhumation of rocks. Geology, 18(12), pp.1173-1177.

Fang, X., Dupont-Nivet, G., Wang, C., Song, C., Meng, Q., Zhang, W., et al., 2020, Revised chronology of Central Tibet uplift (Lunpola Basin). Science Advance v. 6(50), eaba7298. https://doi.org/10.1126/sciadv.aba7298.

Flowers, R.M., Ketcham, R.A., Shuster, D.L., Farley, K.A., 2009, Apatite (U-Th)/He thermochronometry using a radiation damage accumulation and annealing model, Geochim. Cosmochim: Acta, v. 73(8), p. 2347-2365.

Foeken, J., Stuart, F. M., Dobson, K. J., Persano, C., and Vilbert, D., 2006, A diode laser system for heating minerals for (U-Th)/He chronometry: Geochemistry, Geophysics, Geosystems, v. 7, Q04015, https://doi.org/10.1029/2005GC001190.

Gleadow, A.J.W., 1981, Fission track dating methods: What are the real alternatives?: Nuclear Tracks Radiat. Meas., v. 5, p. 3-14, https://doi.org/10.1016/0191-278X(81)90021-4.

Haider, V.L., Dunkl, I., Eynatten, H., v., Ding, L., Frei, D., Zhang, L., 2013, Cretaceous to Cenozoic evolution of the northern Lhasa Terrane and the early Paleogene development of peneplains at Nam Co, Tibetan Plateau. J. Asian Earth Sci. v. 70-71, p. 79–98. https://doi.org/10.1016/j.jseaes.2013.03.005.

Han, Z., Sinclair, H. D., Li, Y., Wang, C., Tao, Z., Qian, X., et al., 2019, Internal drainage has sustained low-relief Tibetan landscapes since the early Miocene: Geophysical Research Letters, v. 46, p. 8741-8752, https://doi.org/10.1029/2019GL083019.

Hetzel, R., Dunkl, I., Haider, V., Strobl, M., von Eynatten, H., Ding, L., and Frei, D., 2011, Peneplain formation in southern Tibet predates the India-Asia collision and plateau uplift: Geology, v. 39, p. 983-986.

Hu, F., Wu, F., Chapman, J. B., Ducea, M. N., Ji, W., & Liu, S., 2020. Quantitatively tracking the elevation of the Tibetan Plateau since the cretaceous: Insights from whole-rock Sr/Y and La/Yb ratios. Geophysical Research Letters, 47, e2020GL089202. https://doi.org/10.1029/2020GL089202.

Hurford, A.J., and Green P.F., 1982, A users' guide to fission track dating calibration: Earth and Planetary Science Letters, v. 59, p. 343-354, https://doi.org/10.1016/0012-821X(82)90136-4.

Hurford, A.J., and Green P.F., 1983, The zeta age calibration of fissiontrack dating: Chemical Geology, v. 1, p. 285-317, https://doi.org/10.1016/S0009-2541(83)80026-6.

Ji, W.Q., Wu, F.Y., Chung, S.L., Li, J.X., and Liu, C.Z., 2009, Zircon U-Pb Geochronology and Hf Isotopic Constraints on Petrogenesis of the Gangdese Batholith, Southern Tibet: Chemical Geology, v. 262, p. 229–245.

Kapp, P., and DeCelles, P.G., 2019, Mesozoic–Cenozoic geological evolution of the Himalayan-Tibetan orogen and working tectonic hypotheses: American Journal of Science, v. 319, p. 159-254.

Kapp, P., Decelles, P. G., Gehrels, G. E., Heizler, M., and Ding, L., 2007, Geological records of the Lhasa-Qiangtang and Indo-Asian collisions in the Nima area of Central Tibet: Geological Society of America Bulletin, v. 119, p. 917-932.

Kapp, P., Murphy, M. A., Yin, A., Harrison, T. M., Ding, L., & Guo, J. (2003). Mesozoic and Cenozoic tectonic evolution of the Shiquanhe area of western Tibet. Tectonics, 22(4). https://doi.org/10.1029/2001TC001332.

Kapp, P., Yin, A., Harrison, T.M., Ding, L., 2005, Cretaceous-Tertiary shortening, basin development, and volcanism in Central Tibet. Geological Society of America Bulletin, v. 117 (7–8), p. 865–878. https://doi.org/10.1130/b25595.1

Ketcham, R.A., 2005, Forward and inverse modeling of low-temperature thermochronometry data: Reviews in Mineralogy and Geochemistry., v. 58(1), p. 275-314, https://doi.org/10.2138/rmg.2005.58.11.

Ketcham, R.A., Carter, A.R., Donelick, A., Barbarand, J., Hurford, A.J., 2007, Improved modeling of fission-track annealing in apatite: American Mineralogist, v. 92(5-6), p.799-810, https://doi.org/10.2138/am.2007.2281.

Lai, W., Hu, X.M., Garzanti, E., Sun, G.Y., Garzione, C., Fadel, M., Ma, A.L., 2019, Initial growth of the Northern Lhasaplano, Tibetan Plateau in the early Late Cretaceous (ca. 92 Ma): Geological Society of America Bulletin, v. 131(11-12), p. 1823-1836.

Laskowski, A. K., Orme, D. A., Cai, F., and Ding, L., 2019, The Ancestral Lhasa River: A Late Cretaceous trans-arc river that drained theproto–Tibetan Plateau: Geology, v. 47, p. 1029–1033. https://doi.org/10.1130/g46823.

Li, C., Zhao, Z., Lu, H., Li, H., 2022, Late Mesozoic-Cenozoic multistage exhumation of the central Bangong-Nujiang suture, central Tibet. Tectonophysics: v. 827, p. 229-268.

Li, Y.L., Wang, C.S., Dai, J.G., Xu, G.Q., Hou, Y.L., Li, X.H., 2015, Propagation of the deformation and growth of the Tibetan–Himalayan orogen: A review, Earth-Science Reviews, v. 143, p. 36–61.

Liu, D.Z., Tao, X.F., Ma, R.Z., Shi, H., Zhu, L.D., and Hu, X.W., 2004, 1:250,000 geological report of Coqin County with geological map [in Chinese]: Chengdu, China, Chengdu University of Technology.

Liu, L., Qiu, J.S., Li, Z., 2013, Origin of mafic microgranular enclaves (MMEs) and their host quartz monzonites from the Muchen pluton in Zhejiang Province, Southeast China: implications for magma mixing and crust–mantle interaction: Lithos, v. 160-161, p. 145–163, https://doi.org/10.1016/j.lithos.2012.12.005.

Liu-Zeng, J., J. P. Tapponnier, Y. Gaudemer, and L. Ding (2008), Quantifying landscape differences across the Tibetan plateau: Implications for topographic relief evolution, J. Geophys. Res., 113, F04018, doi:10.1029/2007JF000897.

Ludwig, K.R., 2001, Isoplot/Ex (rev. 2.49): a geochronological toolkit for Microsoft Excel: Berkeley Geochronology Center: Special Publication, v. 1, p. 1-58.

Ma, A., Hu, X., Kapp, P., Lai, W., Han, Z., & Xue, W., 2020, Mesozoic Subduction Accretion History in Central Tibet Constrained From Provenance Analysis of the Mugagangri Subduction Complex in the Bangong-Nujiang Suture Zone: Tectonics, v. 39(9), e2020TC006144. https://doi.org/10.1029/2020TC006144.

Montgomery, D.R., 1994, Valley incision and the uplift of mountain peaks. Journal of Geophysical Research: Solid Earth, 99(B7), pp.13913-13921.

Murphy, M.A., Yin, A., Harrison, T.M., Dürr, S.B., Chen, Z., Ryerson, F.J., Kidd, W.S.F., Wang, X., and Zhou, X., 1997, Did the Indo-Asian collision alone create the Tibetan plateau? Geology, v. 25, p. 719-722.

Nábělek J, Hetényi G, Vergne J, et al. 2009. Underplating in the Himalaya-Tibet collision zone revealed by the Hi-CLIMB experiment. Science, 325(5946): 1371-1374.

Orme, D., and Laskowski, A., 2016, Basin analysis of the Albian–Santonian Xigaze forearc, Lazi region, south-central Tibet: Journal of Sedimentary Research, v. 86, p. 894-913.

Orme, D., Carrapa, B., Kapp, P., 2015, Sedimentology, provenance and geochronology of the Upper Cretaceous–Lower Eocene western Xigaze forearc basin, southern Tibet: Basin Research, v. 27, p. 387-411.

Persano, C., Stuart, F.M., Bishop, P., Dempster, T.J., 2005, Deciphering continental breakup in eastern Australia using low-temperature thermochronometers: Journal of Geophysical Research, V. 110, B12405, https://doi.org/10.1029/2004JB003325.

Qian, X., Li, Y., Dai, J., Wang, C., Han, Z., Zhang, J., and Li, H. A., 2021, Apatite and zircon (U–Th)/He thermochronological evidence for Mesozoic exhumation of the Central Tibetan Mountain Range: Geological Journal, v. 56(1), p. 599-611.807 https://doi.org/10.1002/gj.3979.

Reiners, P.W., Spell, T. L., Nicolescu, S., Zanetti, K.A., 2004, Zircon (U-Th)/He thermochronometry: He diffusion and comparisons with Ar-40/Ar-39 dating, Geochim. Cosmochim: Acta, V. 68(8), P. 1857-1887.

Rohrmann, A., Kapp, P., Carrapa, B., Reiners, P. W., Guynn, J., Ding, L., and Heizler, M., 2012, Thermochronologic evidence for plateau formation in central Tibet by 45 Ma: Geology, v. 40, p. 187-190.

Sun, G.Y., Hu, X.M., Sinclair, H.D., 2017, Early Cretaceous palaeogeographic evolution of the Coqen Basin in the Lhasa Terrane, southern Tibetan Plateau: Palaeogeography, Palaeoclimatology, Palaeoecology, V. 485, P. 101-118.

Sun, G.Y., Hu, X.M., Sinclair, H.D., Marcelle, B.K., Wang, J.G., 2015a, Late Cretaceous evolution of the Coqen basin (Lhasa terrane) and implications for early topographic growth on the Tibetan Plateau: Geological Society of America Bulletin, v. 127, p. 1001-1020.

Sun, G.Y., Hu, X.M., Zhu, D.C., Hong, W.T., Wang, J.G., Wang, Q., 2015b, Thickened juvenile lower crust–derived ~90 Ma adakitic rocks in the central Lhasa terrane, Tibet: Lithos, v. 224-225, p. 225-239.

Tian, Y.T., Kohn, B. P., Gleadow, A.J.W., and Hu S., 2014, A thermochronological perspective on the morphotectonic evolution of the southeastern Tibetan Plateau: Geophys. Res. Solid Earth, v. 119, p. 676-698, https://doi.org/10.1002/2013JB010429.

Tong, K., Li, Z., Zhu, L., Xu, G., Zhang, Y., Kamp, P. J., Tao, G., Yang, W., Li, J., Wang, Z., Jiang, X., and Zhang, H., 2022, Thermochronology constraints on the Cretaceous-Cenozoic thermo-tectonic evolution in the Gaize region, central-western Tibetan Plateau: Implications for the westward extension of the proto-Tibetan Plateau: Journal of Asian Earth Sciences, 240, 105419.

van Achterbergh, E., Ryan, C.G.., Jackson, S.E., and Griffin, W.L., 2001, Data reduction software for LA-ICPMS: appendix. Laser ablation-ICP-mass spectrometry in the earth sciences: principles and applications: Short Course Series, 29. Ottawa, Ontario, Mineralog. Assoc. Canada, p. 239-243.

Volkmer, J.E., Kapp, P., Guynn, J.H., and Lai, Q., 2007, Cretaceous-Tertiary structural evolution of the north central Lhasa terrane, Tibet: Tectonics, v. 26, TC6007, doi:10.1029/2005TC001832.

Wang, C., Li, X., Liu, Z., Li, Y., Jansa, L., Dai, J., and Wei Y., 2012, Revision of the Cretaceous-Paleogene stratigraphic framework, facies architecture and provenance of the Xigaze forearc basin along the Yarlung Zangbo suture zone: Gondwana Research, v. 22, p. 415–433.

Wang, C., Zhao, X., Liu, Z., Lippert, P.C., Graham, S.A., Coe, R.S., Yi, H., Zhu, L., Liu, S., and Li, Y., 2008, Constraints on the early uplift history of the Tibetan Plateau: Proceedings of the National Academy of Sciences of the United States of America, v. 105, p. 4987-4992.

Wang, Q., Zhu, D.C., Zhao, Z.D., Liu, S.A., Chung, S.L., Li, S.M., Liu, D., Dai, J.G.,Wang, L.Q., Mo, X.X., 2014. Origin of the ca. 90Mamagnesia-rich volcanic rocks in SENyima, central Tibet: products of lithospheric delamination underneath the Lhasa–Qiangtang collision zone. Lithos 198–199, 24–37.

Wei, Y., Zhang, K., Garzione, C.N., Xu, Y., Song, B., Ji, J., 2016, Low palaeoelevation of the northern Lhasa terrane during late Eocene: Fossil foraminifera and stable isotope evidence from the Gerze Basin, Scientific Reports: v. 6, p. 27508.

Xiong, Z.Y, Liu, X.H, Ding, L., Farnsworth A., Spicer, A., Xu, Q., Valdes P., He, S., Zeng, D., Wang, C., Li, Z., Guo, X., Su T., Zhao, C., Wang H., Yue Y., 2022, The rise and demise of the Paleogene Central Tibetan Valley: Science Advances, v. 8, eabj0944.

Xu, Y.W., Hu, X.M., Garzanti, E., BouDagher-Fadel, M., Sun, G.Y., Lai, W., Zhang S.J., 20212022, Mid-Cretaceous thick carbonate accumulation in Northern Lhasa (Tibet): eustatic vs. tectonic control? Geological Society of America Bulletin, v. 134, p. 389–404. doi: https://doi.org/10.1130/B35930.1.

Xue, W.W., Najman, Y., Hu, X.M., Persano, C., Stuart, F.M., Li, W., Ma, A.L., Wang, Y., 2022, Late Cretaceous to Late Eocene exhumation in the Nima area, central Tibet: Implications for development of low relief topography of the Tibetan Plateau: Tectonics, v. 41, e2021TC006989. https://doi.org/10.1029/2021TC006989.

Yang, H.H., Song, Y., Dilles, J.H., Sousa, F., Danisik, M., Yang, C., 2019, The thermaltectonic history of the Duolong ore district: evidence from apatite (U-Th)/He dating. Acta Petrologica Sinica v.35 (3), p. 867–878 (in Chinese with English abstract). https://doi.org/10.18654/1000-0569/2019.03.15.

Zhao, Z., Lu, L., Wu, Z., 2019, Uplifting evolution of the Central Uplift Belt, Qiangtang: constraints from tectonothermochronology. Earth Sci. Front. v. 26, p. 249–263 (in Chinese with English abstract).

Zhao, Z.B., Bons, P.D., Stübner, K., Wang, G.H., and Ehlers, T.A., 2017, Early Cretaceous exhumation of the Qiangtang Terrane during colli-sion with the Lhasa Terrane, Central Tibet: Terra Nova, v. 29, p. 382–391.

Zhu, D.C., Mo, X.X., Niu, Y.L., Zhao, Z.D., Wang, L.Q., Liu, Y.S., and Wu, F.Y., 2009, Geochemical investigation of Early Cretaceous igneous rocks along an east-west traverse throughout the central Lhasa Terrane, Tibet: Chemical Geology, v. 268, p. 298–312.

Zhu, D.C., Pan, G.T., Mo, X.X., Wang, L.Q., Liao, Z.L., Zhao, Z.D., Dong, G.C., and Zhou, C.Y., 2006, Late Jurassic-Early Cretaceous geodynamic setting in middle-northern Gangdese: new insights from volcanic rocks: Acta Petrologica Sinica (in Chinese with English abstract), v. 22, p. 534–546.

Zhu, D.C., Zhao, Z.D., Niu, Y.L., Mo, X.X., Chung, S.L., Hou, Z.Q., Wang, L.Q., and Wu, F.Y., 2011a, The Lhasa Terrane: Record of a microcontinent and its histories of drift and growth: Earth and Planetary Science Letters, v. 301, p. 241–255.

Fig. 1

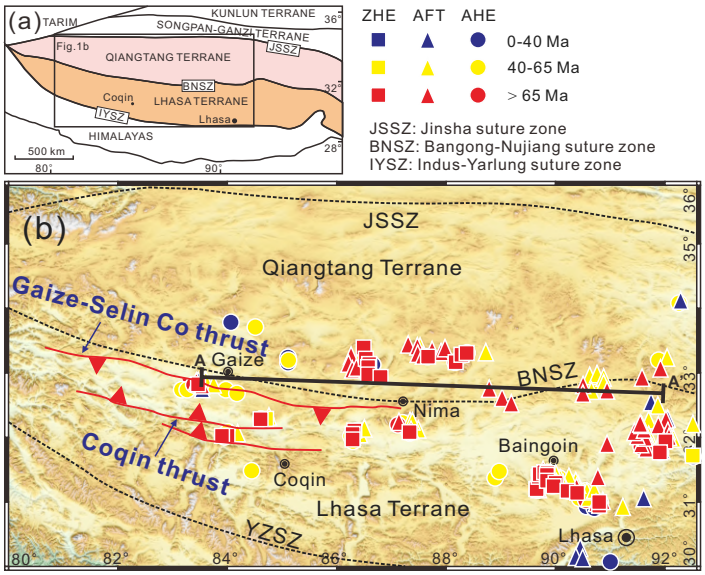
(a)
TARIM
KUNLUN TERRANE
SONGPAN-GANZI TERRANE
Fig.1b
QIANGTANG TERRANE
JSSZ
BNSZ
Coqin
LHASA TERRANE
IYSZ
Lhasa
HIMALAYAS
500 km
80°
90°
36°
32°
28°
ZHE AFT AHE
0-40 Ma
40-65 Ma
> 65 Ma
JSSZ: Jinsha suture zone
BNSZ: Bangong-Nujiang suture zone
IYSZ: Indus-Yarlung suture zone
(b)
JSSZ
Qiangtang Terrane
Gaize-Selin Co thrust
A Gaize
BNSZ
Nima
Baingoin
Coqin thrust
Coqin
Lhasa Terrane
YZSZ
Lhasa
80°
82°
84°
86°
88°
90°
92°
36°
35°
33°
31°
30°

Fig. 2

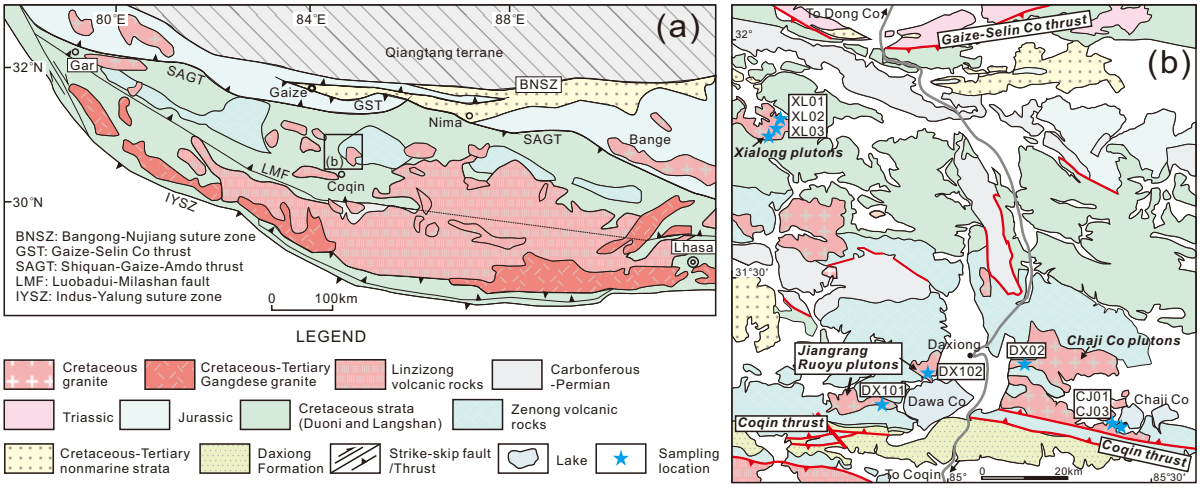
(a)
80°E
84°E
88°E
32°N
30°N
Gar
SAGT
Gaize
GST
BNSZ
Qiangtang terrane
Nima
SAGT
Bange
(b)
LMF
Coqin
IYSZ
Lhasa
BNSZ: Bangong-Nujiang suture zone
GST: Gaize-Selin Co thrust
SAGT: Shiquan-Gaize-Amdo thrust
LMF: Luobadui-Milashan fault
IYSZ: Indus-Yalung suture zone
0 100km
LEGEND
Cretaceous granite
Cretaceous-Tertiary Gangdese granite
Linzizong volcanic rocks
Carbonferous -Permian
Triassic
Jurassic
Cretaceous strata (Duoni and Langshan)
Zenong volcanic rocks
Cretaceous-Tertiary nonmarine strata
Daxiong Formation
Strike-skip fault /Thrust
Lake
Sampling location

(b)
To Dong Co
Gaize-Selin Co thrust
32°
XL01
XL02
XL03
Xialong plutons
31°30'
Jiangrang
Ruoyu plutons
Daxiong
DX02
Chaji Co plutons
DX102
DX101
Dawa Co
CJ01
CJ03
Chaji Co
Coqin thrust
Coqin thrust
To Coqin
85°
0 20km
85°30'

Fig. 3

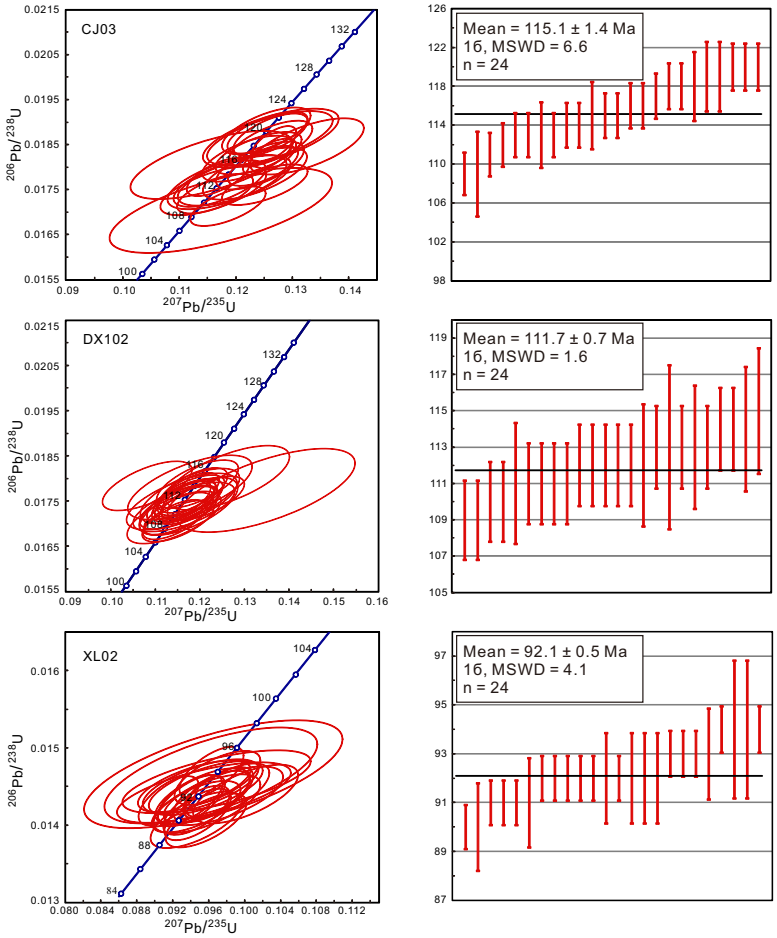
CJ03
Mean = 115.1 ± 1.4 Ma
1σ, MSWD = 6.6
n = 24
DX102
Mean = 111.7 ± 0.7 Ma
1σ, MSWD = 1.6
n = 24
XL02
Mean = 92.1 ± 0.5 Ma
1σ, MSWD = 4.1
n = 24
206Pb/238U
207Pb/235U

Fig. 4

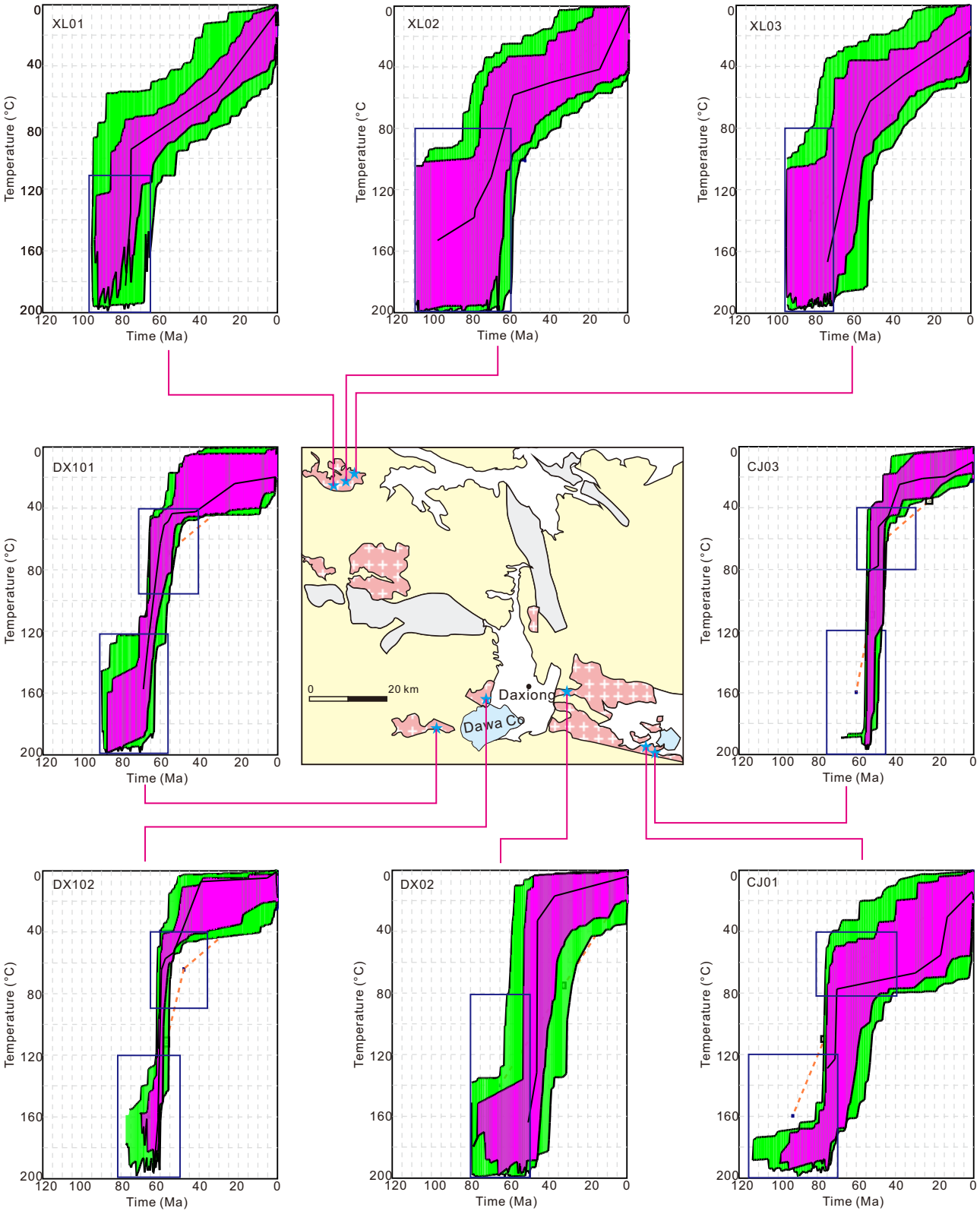
XL01
XL02
XL03
DX101
CJ03
DX102
DX02
CJ01
Temperature (°C)
Time (Ma)
0
40
80
120
160
200
120
100
80
60
40
20
0
0
20 km
Daxiong
Dawa Co

Fig. 5

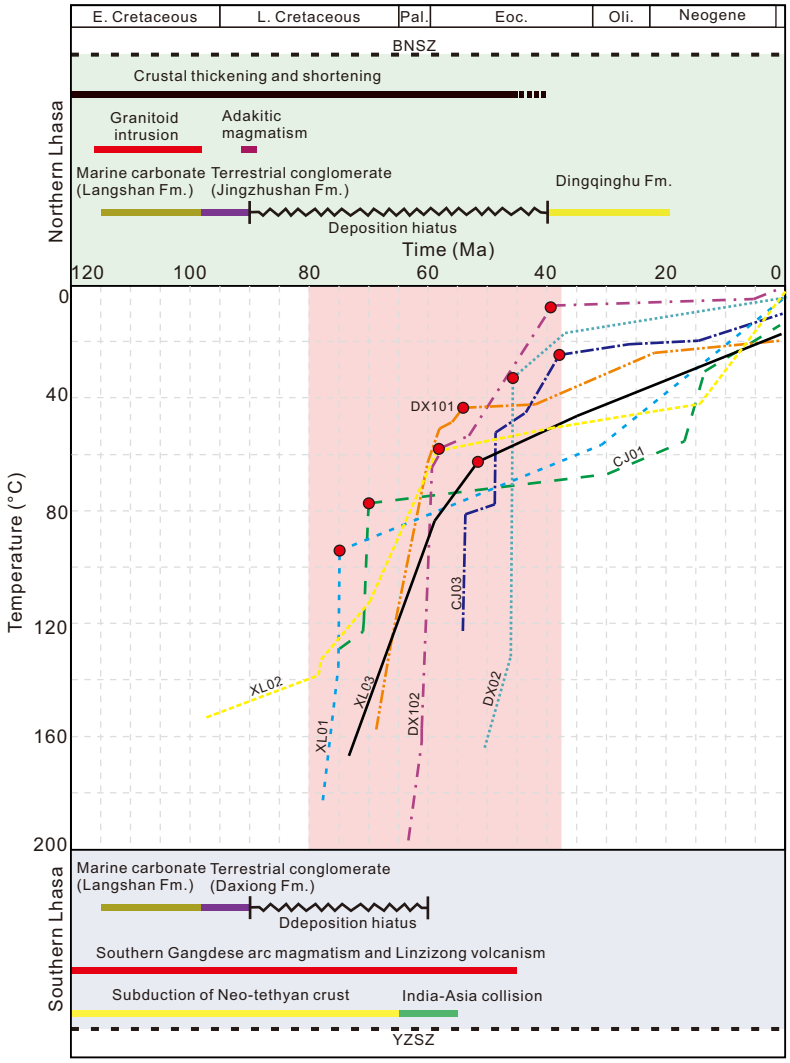
E. Cretaceous
L. Cretaceous
Pal.
Eoc.
Oli.
Neogene
BNSZ
Crustal thickening and shortening
Granitoid intrusion
Adakitic magmatism
Northern Lhasa
Marine carbonate (Langshan Fm.)
Terrestrial conglomerate (Jingzhushan Fm.)
Dingqinghu Fm.
Deposition hiatus
Time (Ma)
120
100
80
60
40
20
0
Temperature (°C)
0
40
80
120
160
200
DX101
CJ01
CJ03
XL02
XL03
XL01
DX102
DX02
Marine carbonate (Langshan Fm.)
Terrestrial conglomerate (Daxiong Fm.)
Ddeposition hiatus
Southern Lhasa
Southern Gangdese arc magmatism and Linzizong volcanism
Subduction of Neo-tethyan crust
India-Asia collision
YZSZ

Fig. 6

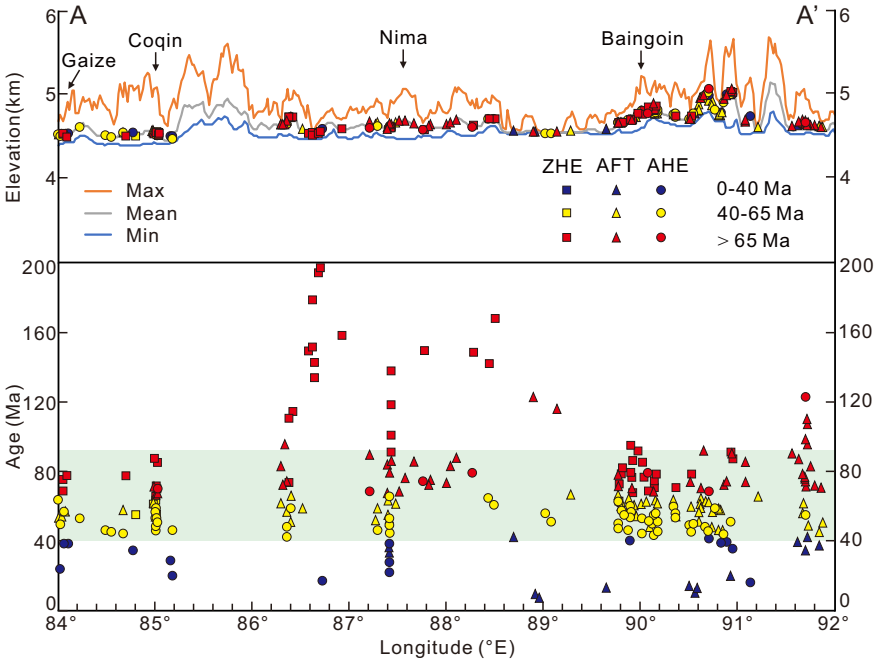
A
A'
Gaize
Coqin
Nima
Baingoin
Elevation(km)
Max
Mean
Min
ZHE AFT AHE
0-40 Ma
40-65 Ma
> 65 Ma
Age (Ma)
Longitude (°E)
84°
85°
86°
87°
88°
89°
90°
91°
92°

Fig. 7

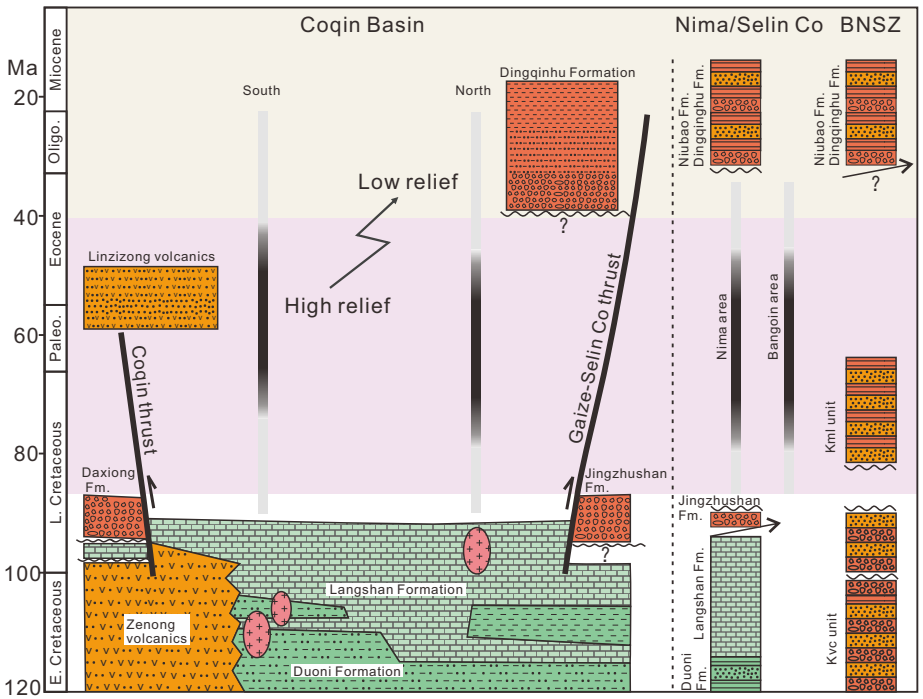
Coqin Basin
Nima/Selin Co
BNSZ
Ma
20
40
60
80
100
120
Miocene
Oligo.
Eocene
Paleo.
L. Cretaceous
E. Cretaceous
South
North
Dingqinhu Formation
Low relief
High relief
Linzizong volcanics
Coqin thrust
Gaize-Selin Co thrust
Daxiong Fm.
Jingzhushan Fm.
Langshan Formation
Zenong volcanics
Duoni Formation
Niubao Fm.
Dingqinghu Fm.
Nima area
Bangoin area
Kml unit
Kvc unit
Langshan Fm.
Duoni Fm.